National University Rail Center - NURail
US DOT OST-R Tier 1 University Transportation Center

NURail Project ID: NURail2020-MTU-R18

Real-time rail defect detection with Eddy Current (EC) technique: signal processing and case studies of rail samples

By

Jiaqing Wang, Ph.D.
Research Assistant
Department of Civil and Environmental Engineering
Michigan Technological University
jiaqingw@mtu.edu

Qingli Dai, Ph.D.
Professor
Department of Civil and Environmental Engineering
Michigan Technological University
qingdai@mtu.edu

Pasi Lautala, Ph.D., P.E.
Associate Professor
Director, Rail Transportation Program
Department of Civil and Environmental Engineering
Michigan Technological University
ptlautal@mtu.edu

08-30-2020

Grant Number: DTRT13-G-UTC52

DISCLAIMER

Funding for this research was provided by the NURail Center, University of Illinois at Urbana - Champaign under Grant No. DTRT13-G-UTC52 of the U.S. Department of Transportation, Office of the Assistant Secretary for Research & Technology (OST-R), University Transportation Centers Program. The contents of this report reflect the views of the authors, who are responsible for the facts and the accuracy of the information presented herein. This document is disseminated under the sponsorship of the U.S. Department of Transportation's University Transportation Centers Program, in the interest of information exchange. The U.S. Government assumes no liability for the contents or use thereof.

NURail2020-MTU-R18

Final Report Aug 30, 2020

TECHNICAL SUMMARY

Title

Real-time rail defect detection with Eddy Current (EC) technique: signal processing and case studies of rail samples

Introduction

Safety is one of the key issues for rail transportation. Nowadays, rails are exposed to constantly increasing traffic with heavy loads and high-speed trains. Increasing the efficiency, frequency, and speed of rail defect detection can reduce maintenance costs and improve operational safety. The non-contact eddy current system can be operated in high train speeds to measure both surface and subsurface flaws. While methods that rely on eddy currents are available, the commercial Eddy Current (EC) system cannot directly provide defect types and patterns. It is generally based on live measurement data and also relies on commercially designed data acquisition devices for signal analysis. In addition, the ability to identify crack types and the possibility of detecting subsurface defects have been of concern with the current commercial EC system. The main objective of this research is to explore the eddy current based methods for inspecting surface/subsurface defects on rails with enhanced performance for defect classification by distinguish the crack depths or crack angles.

In this project, the optimization of eddy current rail inspection technique will be conducted in two phases to test the reliability of defect inspection and the ability for classification of different defect signals; Phase 1 will develop an integrated hardware & software EC measurement system to accurately detect machined cracks in steel samples sample with different crack depths and angles, the effectiveness of the signal differences with defect geometry changes will be investigated ; Phase 2 is a case study on rail samples with different defect types, which will be measured by the established EC rail inspection system and the different defect signals will be compared and collected. Specifically, the ability to identify and characterize the following defects in explored; (1) Surface defects: a) rolling contact fatigue (RCF) cracks, b) Bolt hole crack, c) Rail web longitudinal crack, d) Base dent defect, and d) Gauge corner crack; and (2) Subsurface defects: a) Subsurface rail head defect, b) Subsurface rail web defect, and c) Subsurface gauge corner defect.

Results

1. AE sensor measurement setup and data processing techniques

The eddy current probe (ECP) used in this investigation has a low-frequency operation range from 5kHz to 100kHz, which is advantageous for scanning larger areas and for detecting relatively large flaw sizes [1]. The ECP head diameter is about 6.3 mm (0.25 in.). An alternating current (AC) function generator was used to produce excitation sinewave at a constant frequency of 5kHz [2]. For collecting the signals from the ECP, a NI PCIe 6341 card was used for data acquisition along with a NI SCB-68A terminal block connector. The voltage and current across the EC probe were measured through the analog inputs to the PCI card. Especially for the current measurement, an external shunt high-precision resistor was applied. The voltage across the resistor was measured through the analog input, which was utilized in the Ohm's law for computing the current values. The current and voltage signals from the ECP were then captured simultaneously by two different analog input channels.

With the establishment of the hardware signal acquisition system, the real-time signal processing was developed based on the LabVIEW platform. The DAQmx block acquired the voltage and current of the EC probe with a continuous data sampling rate of 250kHz. Simultaneously, the Fast Fourier Transform (FFT) functions were applied to process real-time impedance signals. In addition, the plots of real and imaginary parts of the impedance were established for real-time monitoring. The established hardware EC system was illustrated as shown in **Fig. 1**.

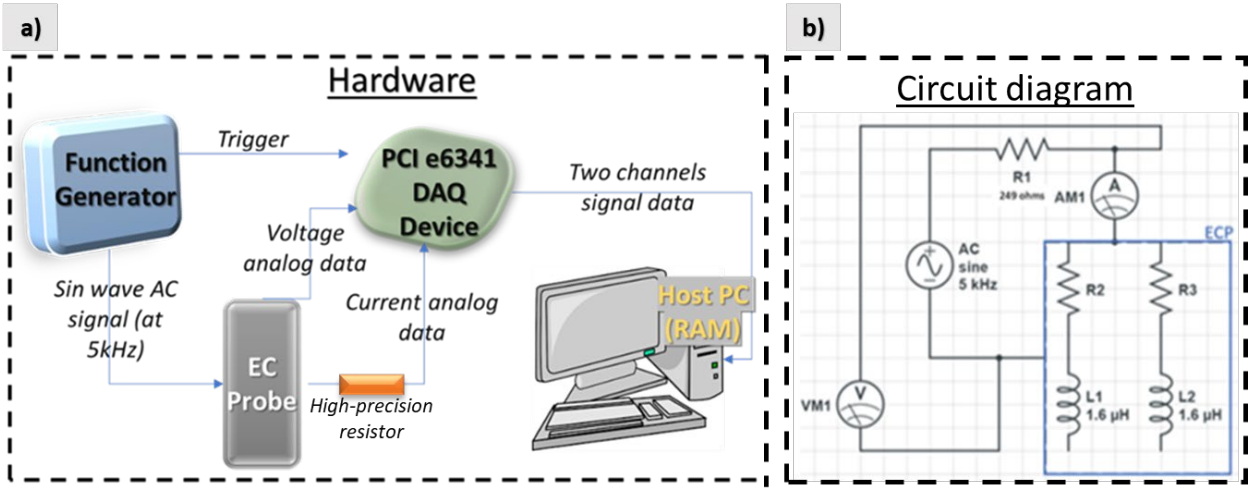

Figure 1 The developed EC inspection system: a) hardware devices; b) circuit diagram of the established EC system

2. PHASE 1-Experimental evaluation of machined cracks on steel sample: the effect of crack depths and orientations on the real-time EC inspection results

Before conducting the experiment, the feasibility of using eddy current to detect machined crack depths and angles needs to be verified. The presence of a material flaw will affect the induced eddy currents in the material and results in the apparent impedance change of the coil. Eddy

currents are more concentrated at the surface and decrease in intensity with distance below the surface of the metal [3]. As shown in equation (1), the standard depth of penetration (d) can be calculated as:

$$d = \sqrt{\frac{\rho}{f\mu_r}} - - - - - - - - - - - - - eq.(1)$$

where δ is the skin depth (mm), μ is the magnetic permeability (H/m), ρ is electrical resistivity (mohm-cm) and f is frequency (Hz).

Based on the steel material properties and the EC excitation frequency of 5kHz, the standard depth (d) can be estimated as 5.7mm, at which eddy current density has decreased to about 37% of the surface density. At three depths (3d), the eddy current density is down to about 5% of the surface density, and this depth of 17.1mm (0.67inch) can be treated as the effective depth [3]. At the same time, the material under test should have a thickness larger than the effective depth, which will make sure the accuracy of the measurement.

Therefore, in this investigation, the machined crack depths (4mm, 8mm, and 12mm) are in the range of effective depth of 17.1mm, which could be able to be detected and classified by the eddy current signals. At the same time, the steel block has a thickness larger than the effective depth. The physical feasibility of the EC measurement on classifying machined crack geometry changes will be verified.

2.1 Preparation of machined cracks

The eddy current crack detection was conducted on an AISI 1018 carbon steel bar with 2in by 3in cross-section and 1 foot long [4]. The crack depths and crack angles are determined based on typical applications for eddy current measurement on the ferromagnetic materials [5, 6], as shown in **Table 6**. The cracks were machined with a band saw at a constant operation speed, where the crack width is the same for all cracking types.

Table 1 The profiles of artificial cracks on a steel block

	Crack 1	**Crack 2**	**Crack 3**
Crack angle	90°	90°	90°
Crack depth	4 mm	8 mm	12 mm
	Crack 4	**Crack 5**	**Crack 6**
Crack angle	75°	75°	75°
Crack depth	4 mm	8 mm	12 mm
	Crack 7	**Crack 8**	**Crack 9**
Crack angle	45°	45°	45°
Crack depth	4 mm	8 mm	12 mm
	Crack 10	**Crack 11**	**Crack 12**

Crack angle	15°	15°	15°
Crack depth	4 mm	8 mm	12 mm

The photographs of the finished steel block with various artificial cracks are as shown in **Fig. 2**.

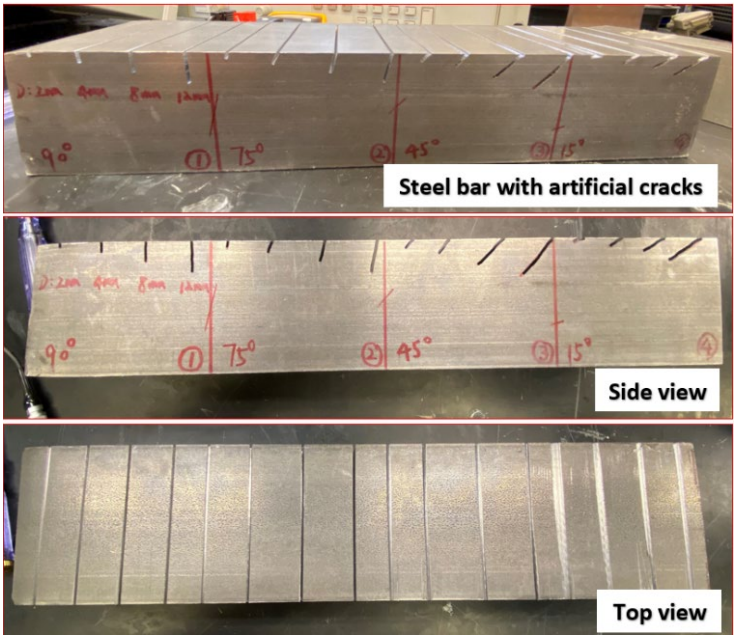

Figure 2 The steel bar with different artificial cracks

The test setup is shown in **Fig. 3** for the eddy current crack signal measurement. The Eddy Current Probe (ECB) is fixed with a fixture to hold it in the vertical position, and the distance between the probe head and the specimen can be fixed to minimize the lift-off effect. In this testing section, there are three cracks measured by following the moving direction. Three cracks are made vertically at 90 degrees with three different depths.

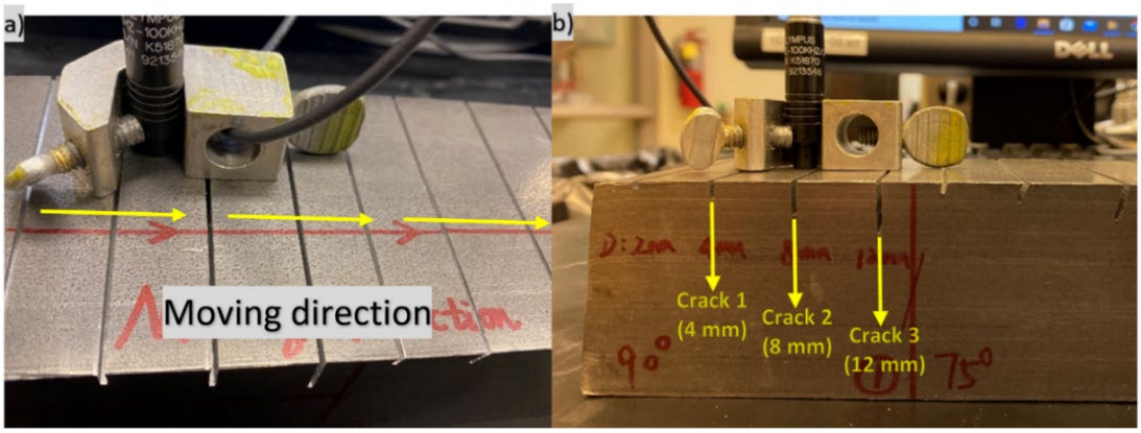

Figure 3 Test setup and inspection of machined cracks

2.2 The effect of crack depths on the eddy current signals

(1) Real-time plots of real and imaginary parts of the impedance

The real-time impedance analyzer was developed along with the simultaneously measured voltage and current signals, as shown in **Fig. 3**. The real part of impedance reflected the real-time resistance change, while the imaginary part of impedance reflected the inductive reactance change, which are represented as shown in **Fig. 4a)** and **Fig. 4b)**, respectively. From these two waveform charts, the obvious change in the signals can be found when the sensor moved on these cracks. Besides, the peak values were also increased with crack depths.

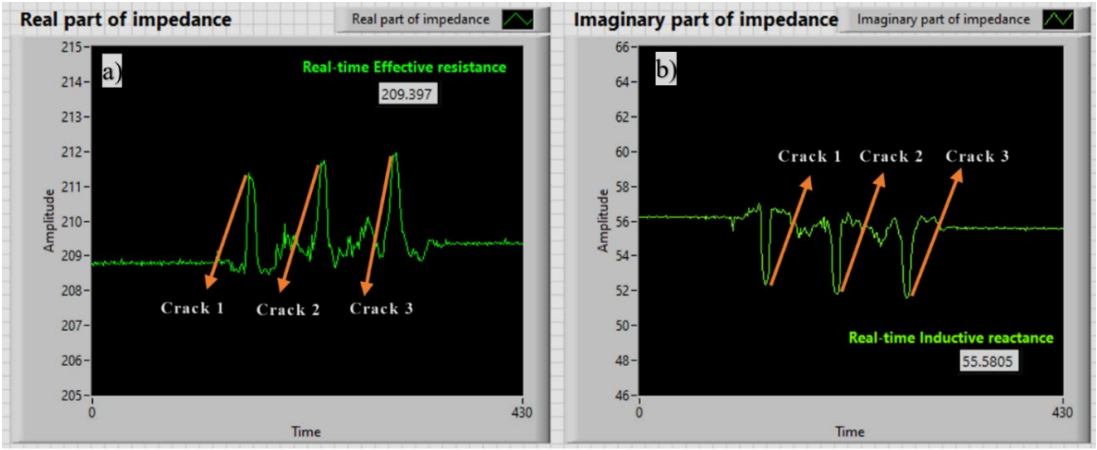

Figure 4 The real-time impedance analyzer plot of cracks with different depth at 90-degree: a) and b) Real part and Imaginary part of impedance changing with time

(2) Normalized impedance plan plots

To analyze the data in detail from the measured signals, the MATLAB data processing code has been developed based on the relative impedance changes between flawless surface positions and different crack positions. The normalized impedance plane plot at 90 degree is shown in **Fig, 5a)**. When the crack orientation changes, the depth in the vertical direction of cracks below the surface will also be changed. The normalized impedance plot at 75 degree is then plotted in **Fig. 5b).** The equations for calculating the normalized impedance plane are illustrated below [12]:

$$X_{cn} = \frac{X_c}{X_0} - - - - - - - - - - - eq.(2)$$

and,

$$R_{cn} = \frac{R_c - R_0}{X_0} - - - - - - - - - eq.(3)$$

where, X_0, R_0 are the inductive reactance and resistance when the sensor placed in air, respectively; X_c, R_c are the new inductive reactance and resistance when the sensor placed on working surface, respectively; X_{cn}, R_{cn} are the normalized inductive reactance and normalized resistance. When the sensor in air condition, $X_{cn} = 1, R_{cn} = 0$.

In eddy current inspection, when the EC probe is placed on the steel block, which is a magnetic material, the eddy current forms in the steel block. The energy of the coil in the EC probe was

dissipated and thus resulting in increased resistance as shown in the flawless work surface [2]. However, with the presence of a crack, the induced eddy current will be obstructed. With increasing crack depth, more eddy currents flow will be affected in the testing piece. This effect leads to the reduction of the secondary magnetic field from the eddy currents [7]. As shown in Figure 5 (a) and (b), with cracks orientated in 90 degree and 75 degree, both the relative reactance X_{cn} and resistance R_{cn}decreased with increasing crack depths. These values were also compared with the data from flawless surface (indicated with the black color).

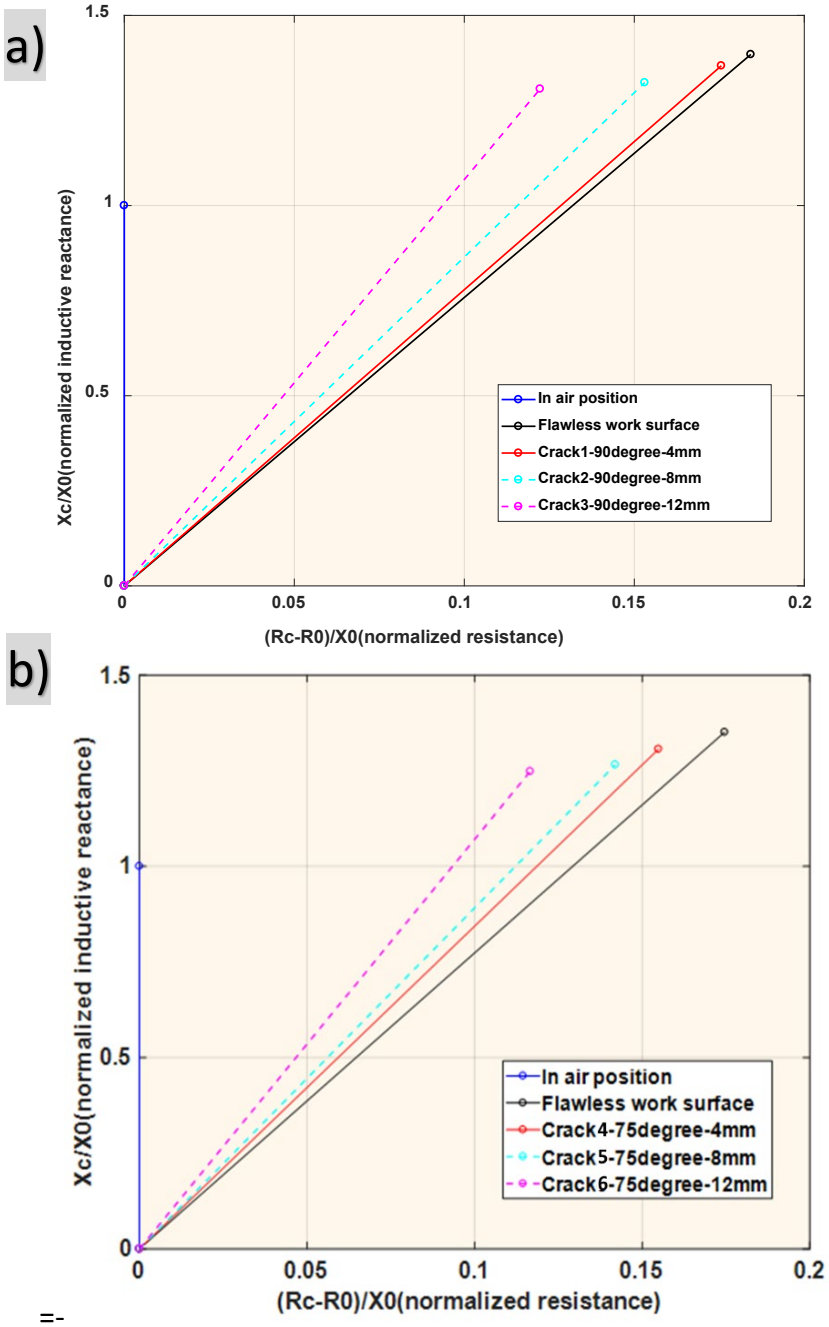

=-

Figure 5 The normalized impedance plane of cracks with different depths: a) at 90 degree; b) at 75 degree

2.3 The effect of crack angles on the eddy current signals

(1) Real-time plots of real and imaginary parts of the impedance

Besides the crack depth effect, the crack orientation effect was examined in this section. As an example, the real-time impedance of cracks with different angles but the same depth of 4mm is shown in **Fig. 6**. It can be observed that the real and imaginary parts of the impedance were changed with the crack angle differences during the EC inspection.

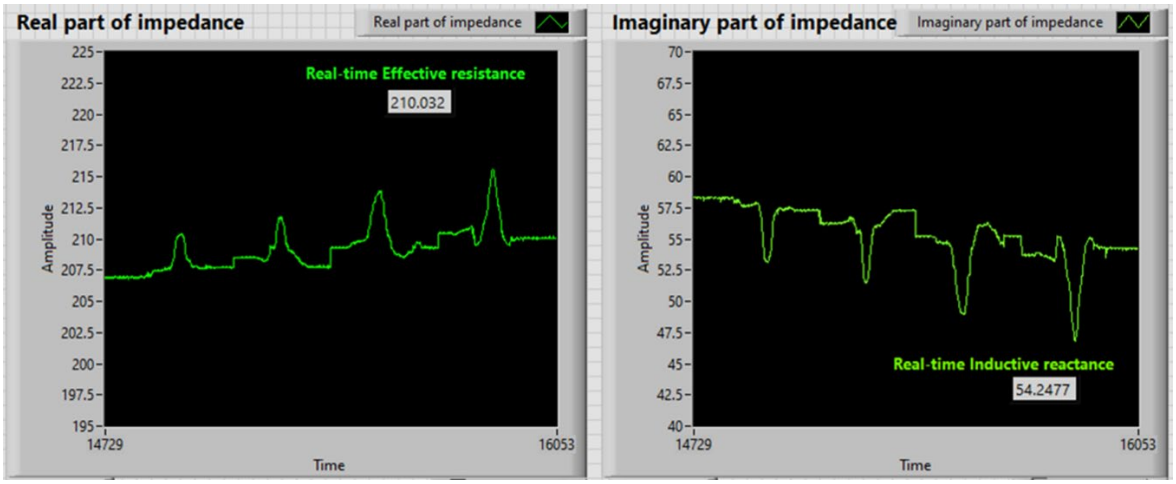

Figure 6 The real-time impedance analyzer plot of cracks with different angles at 4mm depth: a) and Real part and b) Imaginary part of impedance changing with time

(2) Normalized impedance plan plots

The normalized impedance plane was analyzed at different crack angles at 4mm and 8mm depths, as shown in **Fig. 7a)** and **Fig. 7b)**, respectively. It could be verified that the magnitude and phase of the impedance will be changed with the variations of crack angles.

To analysis the results shown in different angles, it can be observed that the 90 degree (vertical crack) represented the smallest effect on the normalized impedance when compared with a flawless surface. However, when the crack direction approached to be parallel to the detection surface, the effect was enlarged. With the crack angle changed from 90 degree to 15 degree, the crack was close to the detection surface, which obstructed more eddy currents that concentrated near the surface, which lead to the reduced induction resistance and reactance as shown in Figure 7 (a) and (b). Therefore, both the relative induction resistance R_{cn} and relative reactance X_{cn} decreased when the crack angles changed from 90 degree to 15 degree.

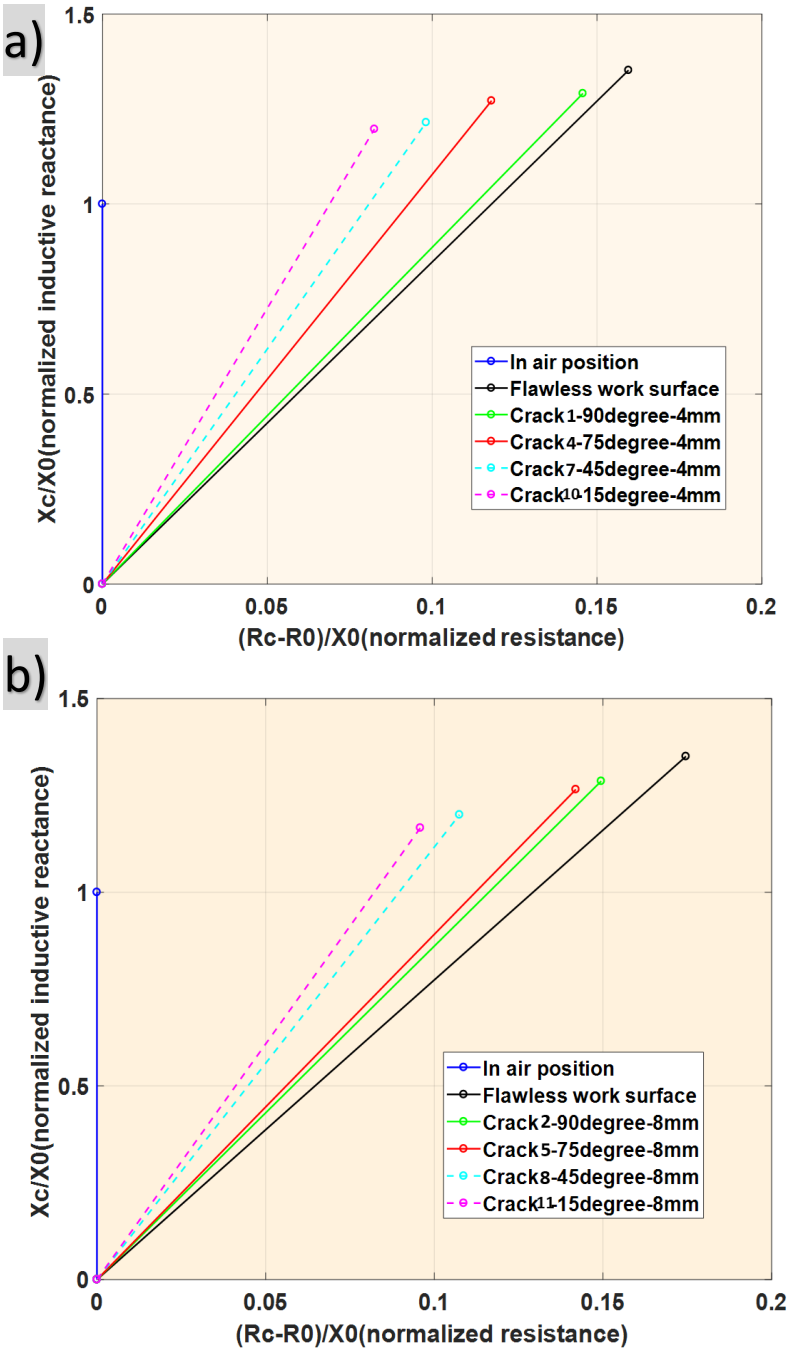

Figure 7 The normalized impedance plane of cracks with different angles: a) at 4mm depth; b) at 8mm depth

Summary of effects of crack depth and orientation of machined cracks on EC signals

In the phase 1 study, the effects of crack depths and angles on the impedance signal changes were investigated. The feasibility of using eddy current to detect and classify crack depth is verified based on the improved EC system. The impedance signal represented some

characterizations with the crack geometry changes. There are some findings can be summarized as below:

(1) During the depths of cracks changed from 4mm to 8mm and 12mm, the measured impedance signal including both the relative induction resistance R_{cn} and reactance X_{cn}decreased with the increasing of crack depths. These results were also compared with the data from the flawless surface location.

(2) During the degree of cracks changed from 90 degree to 75 degree, 45 degree, and 15 degree, both the normalized induction resistance R_{cn} and induction reactance X_{cn} decreased. The 15gree crack generated the most considerable effect on the normalized impedance. When the crack direction approached the detection surface, more induced eddy currents will be obstructed by the crack, which will generate a more considerable effect on the impedance since eddy currents represented higher intensity near the surface.

According to these investigation results, the developed EC system showed potential for classifying cracks with different depths and angles. The further investigation of rail track samples will be conducted in PHASE 2 to validate the capability of the EC inspection system.

3. PHASE 2 Case study in surface/subsurface defects inspection on rail samples based on the established system

In phase 2, the established system was used to detect surface/subsurface defects on rail samples obtained from CN Rail. The capability of the established EC system for measuring rail defects with different geometries was evaluated. The inspection results demonstrated that the defect signals changed with different defect classifications and the crack geometries. Within the same defect type, the geometry differences can be characterized by the defect signal changes as represented in the normalized impedance plane. The detailed measurement results and analysis will be discussed in the following sections.

3.1 EC detection on rolling contact fatigue (RCF) defects

The rolling contact fatigue (RCF) defect is caused by cyclic loading, which is represented as early fatigue damage called crack-like flaws, as shown in **Fig. 8**. By further loading, these crack-like flaws can grow to more significant cracks and cause fractures, such as rail breaks [8]. Thus, the severity of the RCF defects should be able to be determined during the EC inspection.

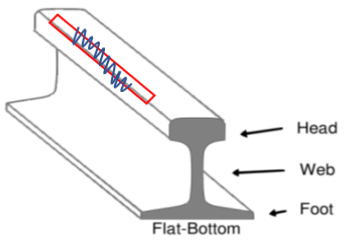

Figure 8 Locations of the RCF defects on the inspected rail samples

In this investigation, two types of RCF defects with different severity were observed and inspected by the established EC system on two rail samples as shown in **Fig. 9**.

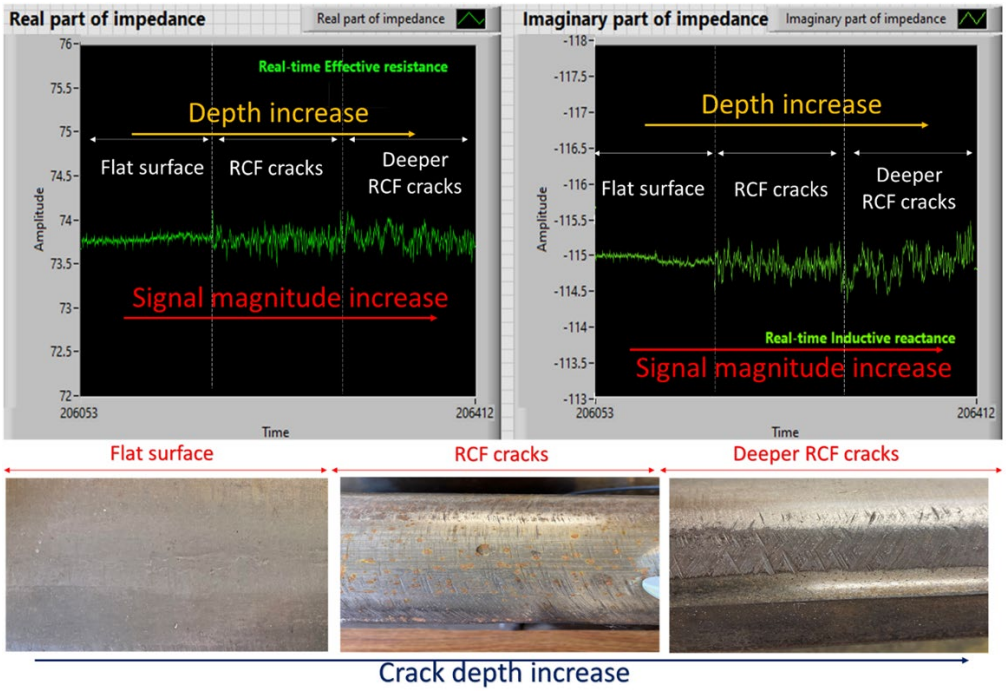

Figure 9 Inspection of RCF cracks on rail head with different depth

The impedance signal showed an almost flat line when the sensor moved on the flawless surface of the rail sample, which can be used as the base line for measuring the crack severity compared with defect signal magnitude changes. It can be noticed that the impedance signals showed an obvious change in RCF defect areas when compared with that of the flawless surface. In addition, with the increase of RCF defect severity, the signal also showed different magnitudes and waveforms. For instance, the signal magnitude difference of inductive reactance was increased from 0.25 Ω to 0.5 Ω when the RCF defect depth increased. This suggests that eddy current might be able to provide some level of quantitative evaluation of RCF.

3.2 EC detection on surface defects of rail samples

3.2.1 Bolt hole crack at rail web

Some cracks can develop from the bolt hole at the rail web due to stress concentration, and these cracks could cause rail web fracture if not detected and repaired adequately at the early stage [9]. In this investigation, a very tiny crack that developed from the bold hole at rail web was inspected by the established EC system, the location of the crack is shown in **Fig. 10**.

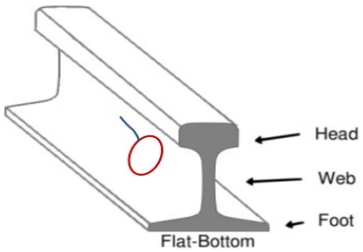

Figure 10 The location of the bolt hole crack

As shown in **Fig. 11**, the bolt hole crack is very tiny, with only 0.12mm width. As shown in the impedance signal results, the magnitude of the signal showed a

small peak jump when the EC probe passed the tiny crack. This result demonstrated that the capability for detecting very early-stage cracks by the established system. The relatively low working frequency at 5kHz is also adequate for capturing small surface cracks.

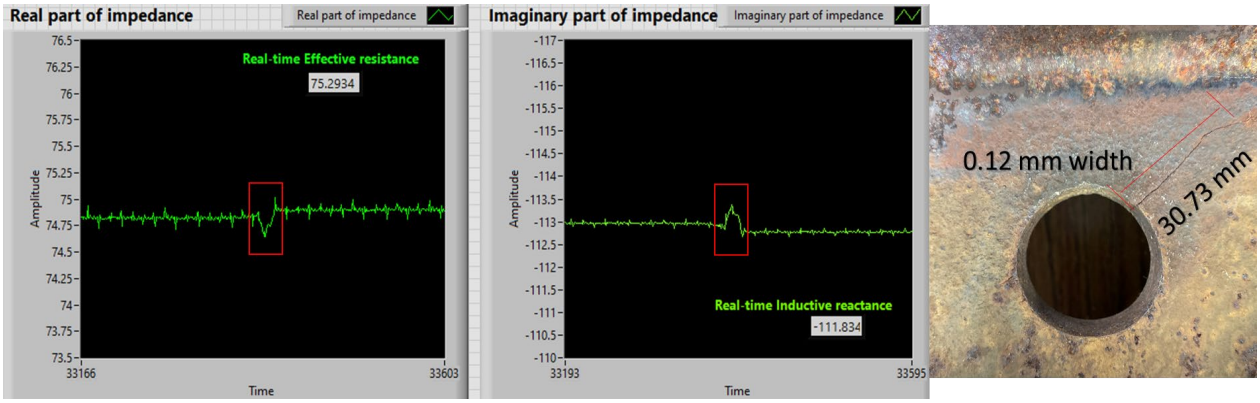

Figure 11 Inspection results of bolt hole crack

3.2.2 Gauge corner surface defect

As shown in **Fig. 12**, a surface crack at the gauge corner with increasing crack depth was inspected by the EC system by moving the sensor along the crack.

The inspection results (**Fig. 13)** showed that signal continuously changed with the increased crack depth and width along the sensor moving direction. This result indicated the good sensitivity of the established system for detecting crack geometry change, as the defect signal peak increased with the crack depth. The impedance signal magnitudes of real and imaginary parts were continuously recorded along the crack.

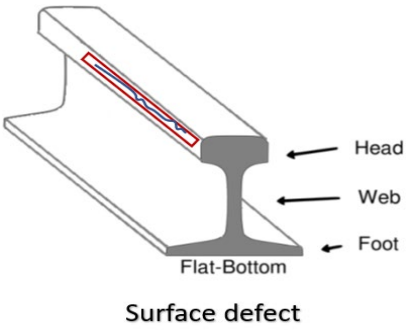

Figure 12 A surface crack at the gauge corner

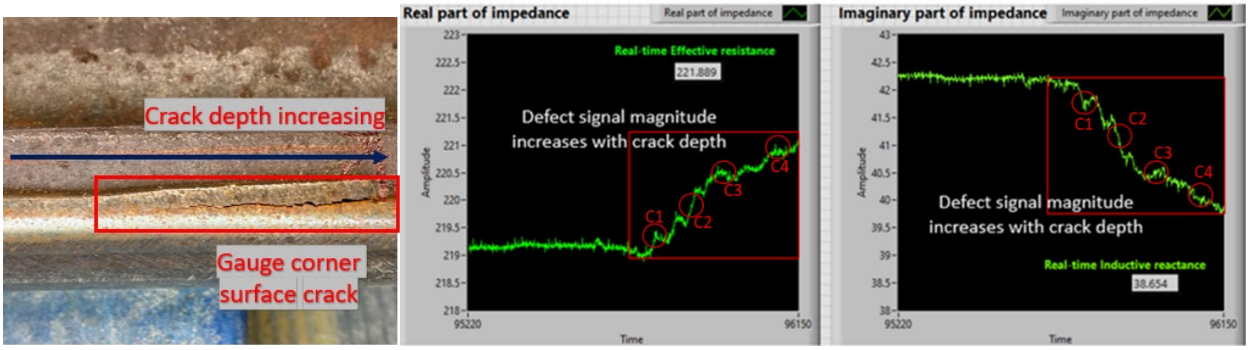

Figure 13 The inspection results of the gauge corner surface crack

The normalized impedance plane plot was processed based on the measured signal impedance changes, which is shown in **Fig. 14**. It can be observed from the normalized impedance plane that the magnitude and phase kept changing during the sensor movement with increasing crack

severity. With the increased crack depth and width, both the normalized induction resistance R_{cn} and induction reactance X_{cn} decreased. Therefore, the normalized phase plots shown in Figure 14 indicated the induction magnetic field changes with increased crack severity (from C1 to C2 to C3 to C4).

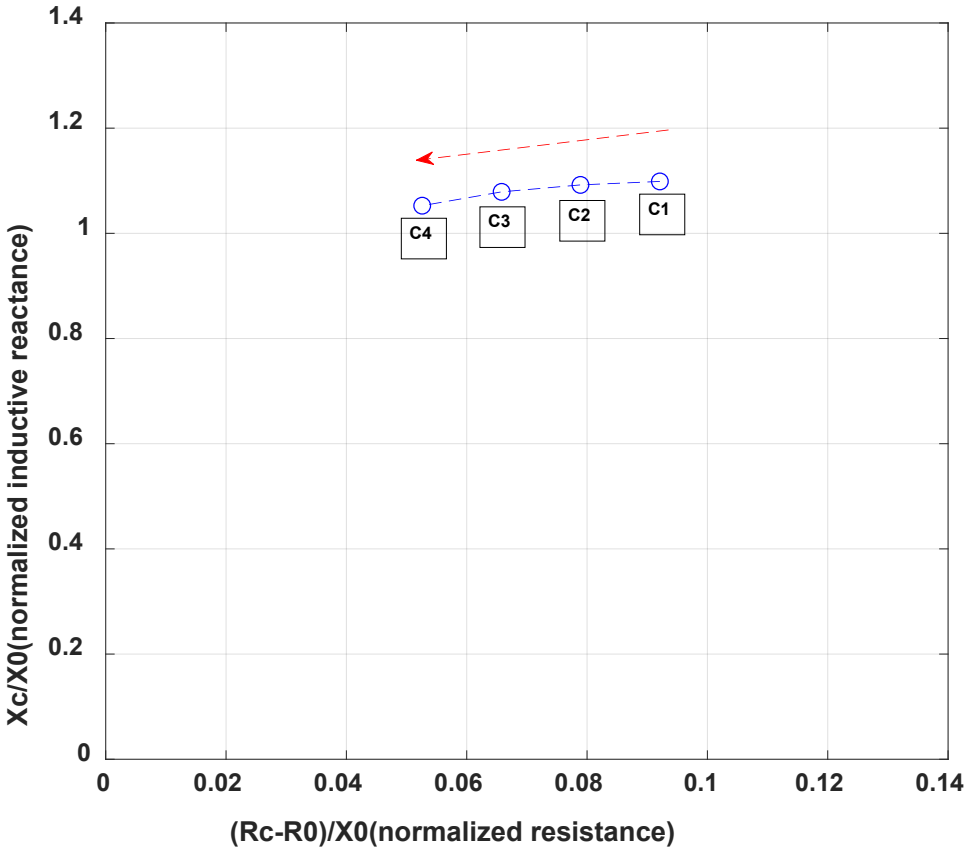

Figure 14 The normalized impedance plane plot during the sensor movement

3.2.3 Surface rail web defects

A longitudinal crack at the rail web was observed and detected by the EC system as shown in **Fig. 15**. Four different locations were selected along the split web crack, where the visual observation cannot accurately distinguish the crack depth changes. The inspection results at four different locations are shown in **Fig. 16**, it can be found that the signal magnitude represented different characterization at different locations. The crack depth change can be reflected by the impedance changes among these four locations.

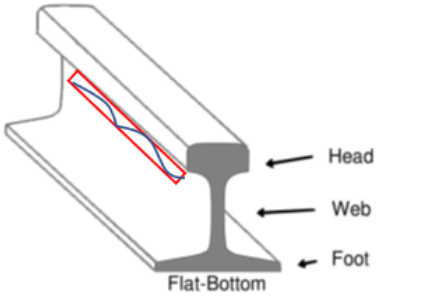

Figure 15 The location of the split web crack

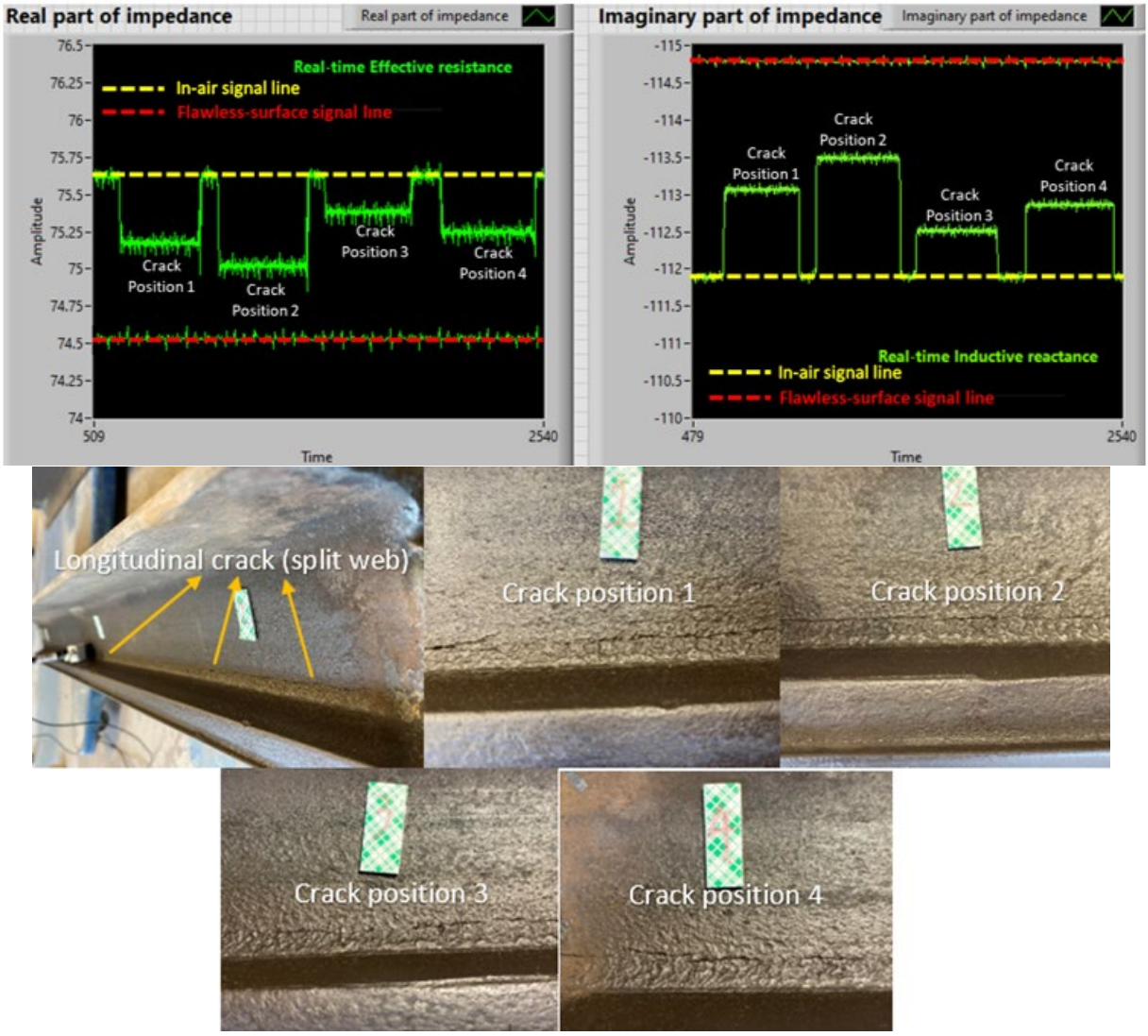

Figure 16 The measurement results at four different locations of the longitudinal split web surface crack

The normalized impedance plane was processed to compare the difference between four different crack locations, as shown in **Fig. 17**. **I**t can be observed that the signal magnitude and the phase were different at four crack locations. Based on the trend that was observed in the machined cracks and rail gauge corner crack. It can be estimated from the normalized impedance plane that the crack position-3 has the largest depth, while the crack-position 2 has the smallest depth.

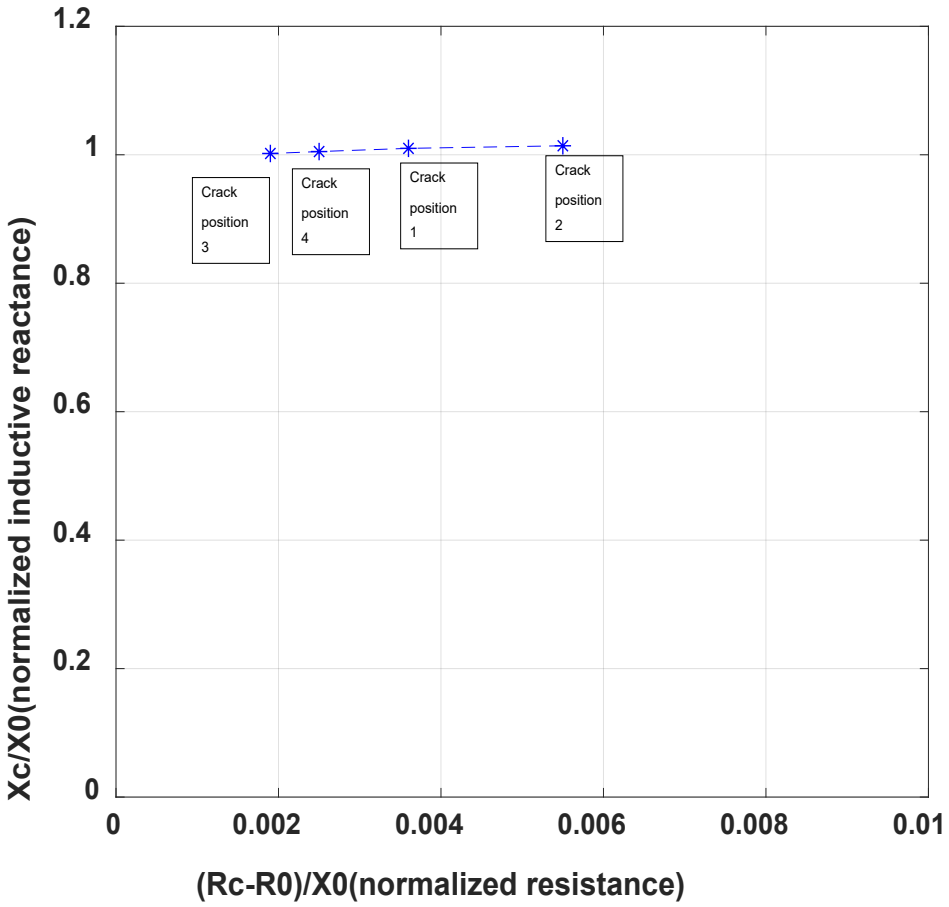

Figure 17 Normalized impedances at four different crack positions of web surface split crack

3.2.4 Surface base defects

With the successful application of the developed EC inspection system on the rail head and rail web, the ability for detecting defects at the rail base was also examined. As shown in **Fig 18**, a surface dent at the base was observed on a rail sample.

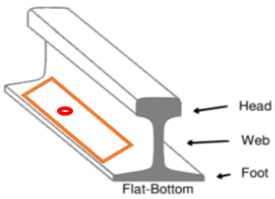

Dent defect on surface of rail base

Figure 18 The surface dent at rail base

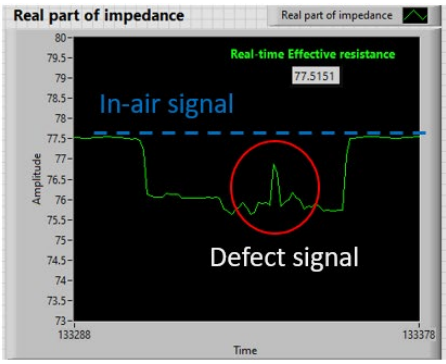

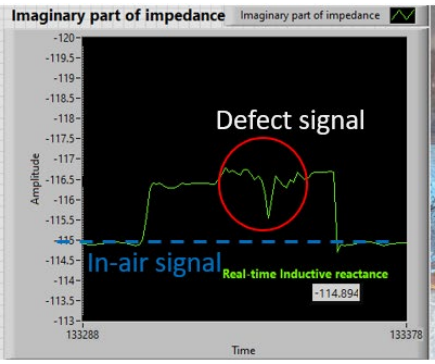

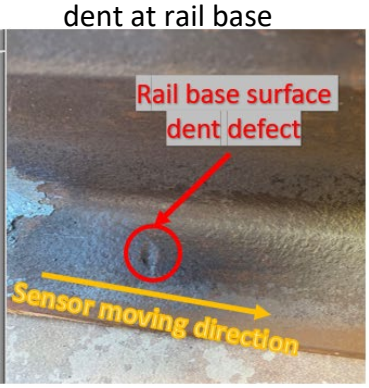

Figure 18 The inspection results on the base surface dent

The monitored signal changes during the sensor movement were recorded(**Fig. 19).** We observed that the signal showed flat line when the sensor on flat base surface, and an obvious peak change about 1.2Ω show off when the sensor passed the dent area.

3.3 EC detection on subsurface defects of rail samples

It is well known that the subsurface defects are hard to be inspected by visual inspection. Thus, the capability of the established system for measuring near-surface subsurface defects at rail samples was illustrated. Many studies have verified that the EC has the ability to detect subsurface defects as long as the defects are located in the range of effective penetration depth [10]. Once the flaw exists in the subsurface zone of the rail, the induced eddy current will be disturbed and the impedance of the coil will be affected [11]. The developed EC system had an excitation frequency of 5kHz. It has been illustrated before that the effective penetration depth at 5kHz is about 17mm for steel material. Therefore, all the subsurface defects in the depth of less than 17mm below the rail surface could be detected by the developed system.

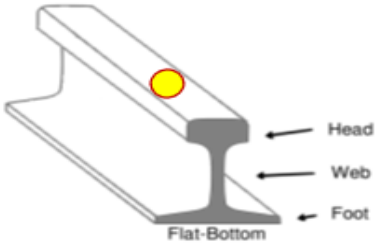

Internal defect, no crack on surface

Figure 20 The location of rail head internal defect

3.3.1 Subsurface defect at rail head

The subsurface rail head defect was observed and detected in this investigation by the established EC system. As shown in **Fig. 20**, the location of the detected rail head subsurface defect was illustrated. Based on visual inspection, we believe this to be caused by material changes due to weld

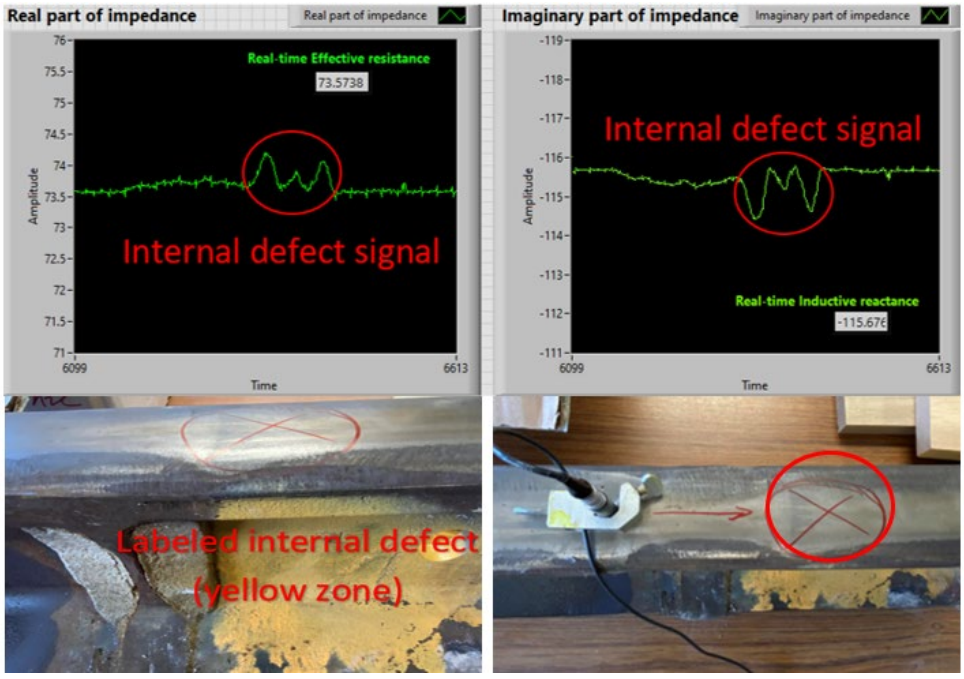

Figure 19 The detection results of rail head subsurface defect

The rail sample from the CN railway had been detected by the ultrasonic device and labeled with yellow paint, which indicated that the yellow zone had subsurface defects, as shown in **Fig. 21**. The signal showed obvious three magnitude peaks (two larger peaks on two sides, one smaller peak in center) when the sensor passed through the subsurface defect area on the rail head, which indicated that the position of the subsurface defect and also the geometry changes inside the subsurface defect.

3.3.2 Subsurface defect at gauge corner

Besides the rail head subsurface defect, a subsurface defect signal was also observed at the gauge corner of a rail sample **Fig. 22**. The signal magnitude showed an obvious jump when the sensor head experienced the suspected subsurface defect location, as shown in **Fig. 23**. The defect signal suggested a subsurface flaw within the range of the effective penetration depth.

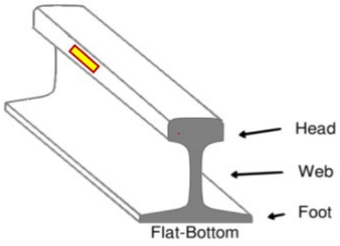

Figure 22 The internal defect at the gauge corner

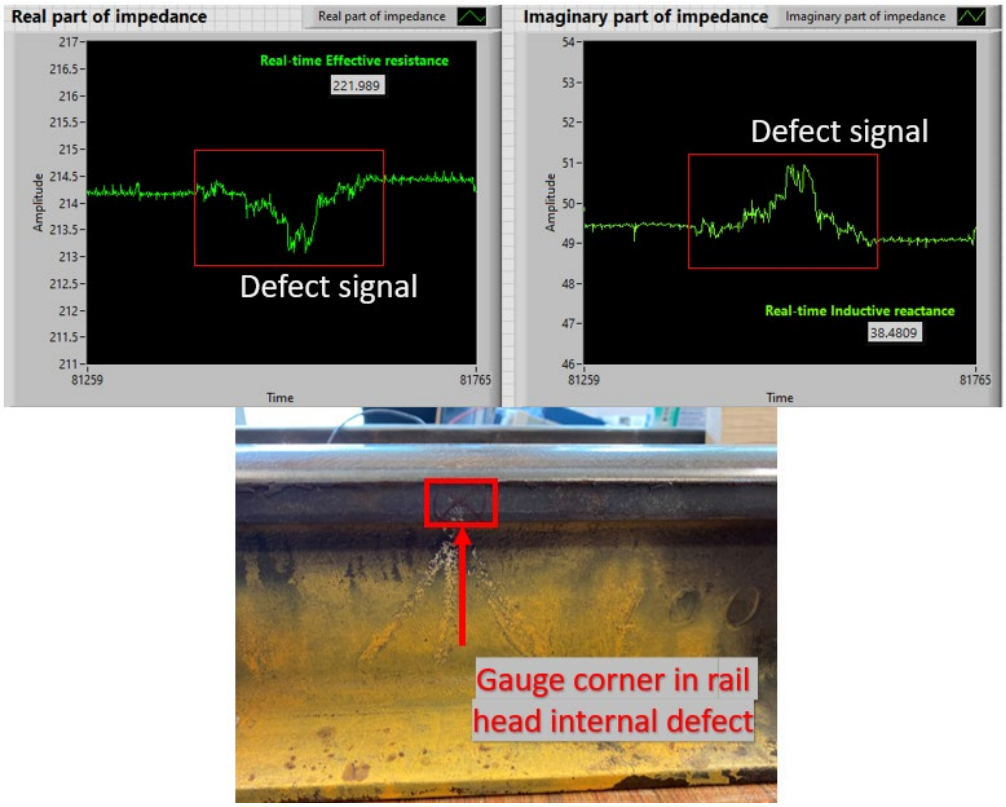

Figure 23 Inspection results of the subsurface gauge corner defect

3.3.3 Subsurface defect at rail web

A subsurface defect at the rail web was also discovered, as illustrated in **Fig. 24**. It can be observed that the signal magnitude changes and the waveform showed distinct behavior when compared with that of other types of defects, as shown in **Fig. 25**.

From these measurements on subsurface defects, it can be found that both the real part and imaginary part of the impedance were changed when the sensor passed the subsurface flaw. The real part of the impedance signal represents a magnitude difference between 0.5-2.0 Ω, whereas the imaginary part of the impedance signal represented a magnitude difference between 1.0-2.5 Ω.

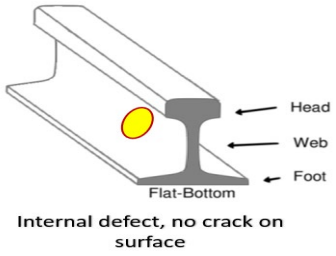

Figure 24 The internal defect at rail web

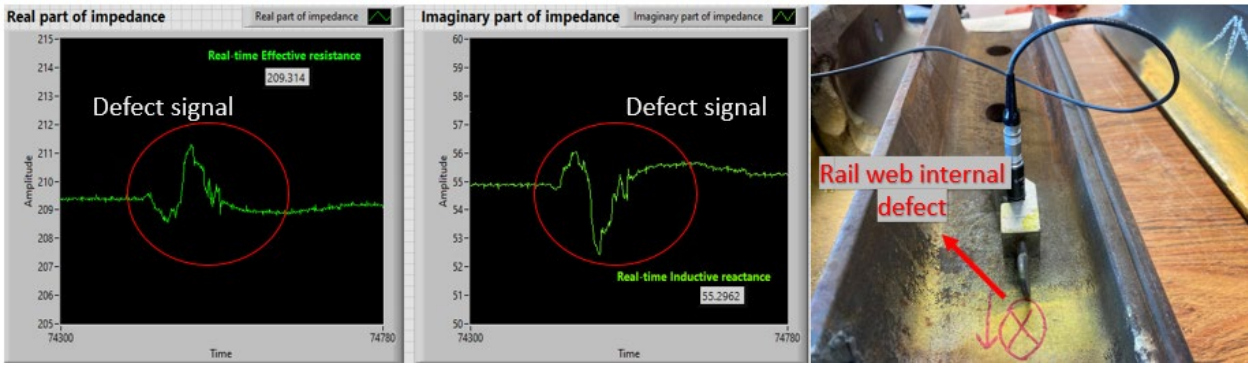

Figure 20 The inspection results of the rail web subsurface defect

3.4 Comparison of EC signals for subsurface and surface defects

The normalized impedance of surface and subsurface defects signals was first compared in the rail head, as shown in **Fig. 26a)**. At rail head, the subsurface defect represented a decreased normalized resistance (R_{cn}) than that of rail head surface RCF, while the normalized reactance (X_{cn}) is almost the same as that of the RCF. Similarly, as shown in **Fig. 26b)**, the normalized impedance of surface and subsurface defects in the gauge corner were compared. The subsurface gauge corner defect generated a reduced R_{cn} and a slightly increased X_{cn} by comparing with that of the surface gauge corner crack. These results indicated the subsurface crack can contribute to the inductive reactance. Since the EC signal is very sensitive to the surface layer, the surface shape and texture of measured samples can also affect the impedance resistance changes.

The normalized impedance of surface and subsurface defects signals was demonstrated in the rail web, as shown in **Fig. 26c)**. The subsurface detection results showed a larger R_{cn} on the normalized impedance when compared with that of the web surface defect. Also, the X_{cn} of subsurface defect was also increased by comparing that of the web surface defect. These defect signals also demonstrated that the subsurface defects can increase the inductive reactance.

a)

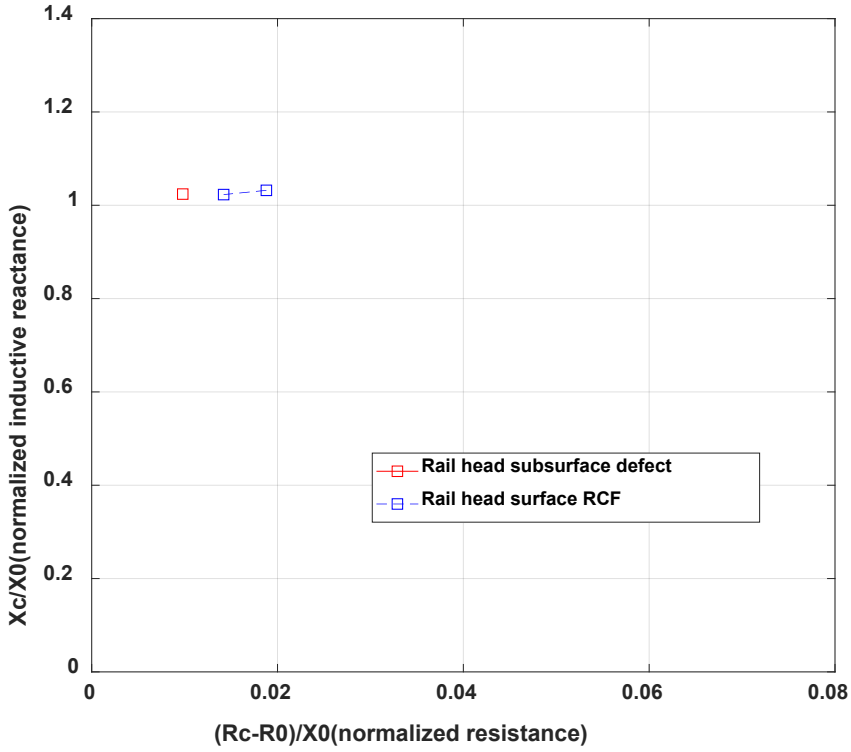
1.4
1.2
1
0.8
0.6
0.4
0.2
0
0
0.02
0.04
0.06
0.08
Xc/X0(normalized inductive reactance)
(Rc-R0)/X0(normalized resistance)
Rail head subsurface defect
Rail head surface RCF

b)

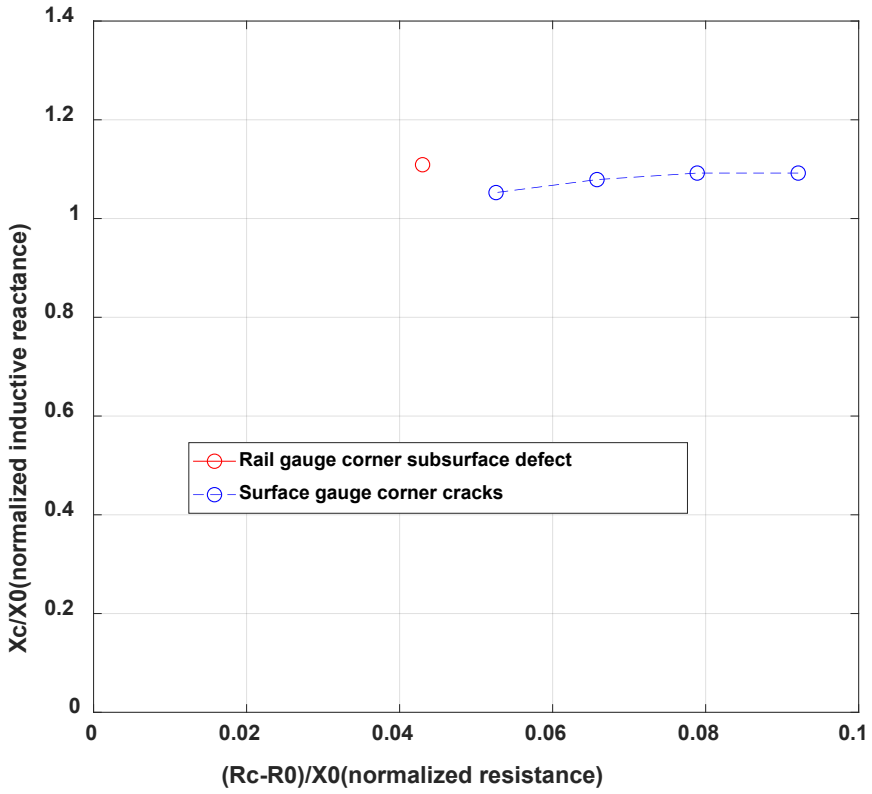
1.4
1.2
1
0.8
0.6
0.4
0.2
0
0
0.02
0.04
0.06
0.08
0.1
Xc/X0(normalized inductive reactance)
(Rc-R0)/X0(normalized resistance)
Rail gauge corner subsurface defect
Surface gauge corner cracks

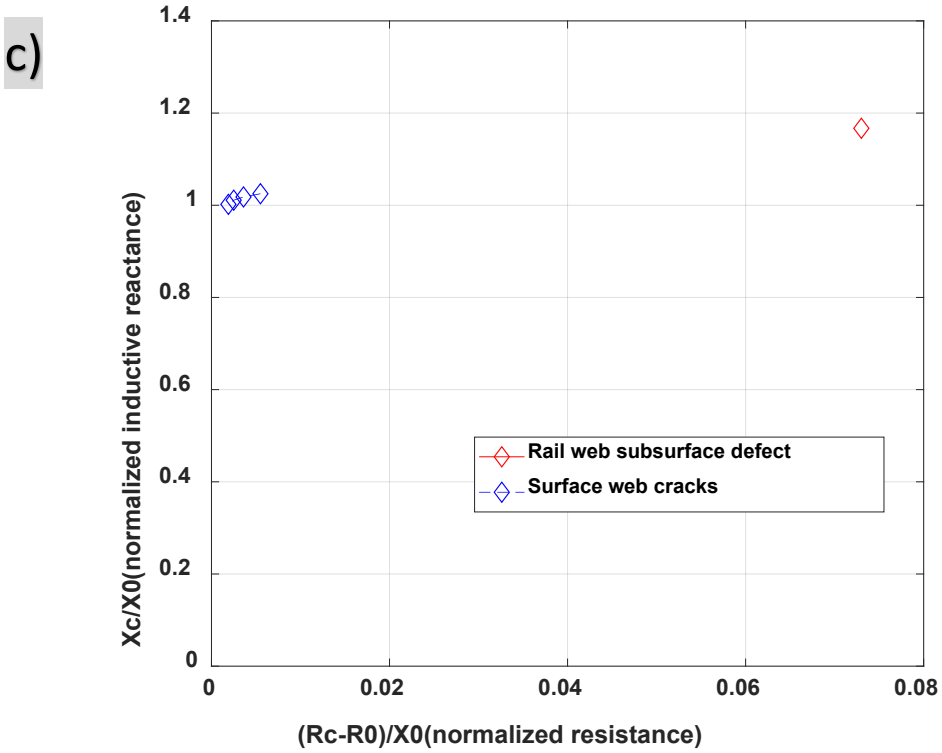

Figure 21 The comparison between surface cracks and subsurface defects: a) defects at rail head; b) defects at rail gauge corner; c) defects at rail web

Summary of EC measurement result on different defects on rail samples

Laboratory tests of defective rail samples were used to demonstrate the ability of our developed system to detect surface/subsurface defects. Also, some differences of parameters were observed with different rail damage scenarios, as summarized below:

(1) The established EC system has good sensitivity to surface texture-like RCF defects. The severity of the RCF defects can be captured by the EC system with impedance changes. Also, if defects exist underneath the RCF and within the effective EC penetration depth, the system may indicate the signal differences but the surface effects are more significant.

(2) Different defects on rail head, gauge corner and rail webs were measured with the EC detection system and the changes of signal waveforms showed good sensitivity. Different defect damage pattern was also indicated with the EC impedance signal changes.

(3) The crack depth or size changes of surface cracks can be represented by the normalized impedance changes, which showed a trend similar to that of machined cracks when the rail surface cracks geometry changes. In general, both the normalized induction resistance R_{cn} and induction reactance X_{cn} were affected more with the increase of crack severity.

(4) The subsurface defects were detected in rail head, gauge corner, and rail web and their impedance phase plots were compared. The signal impedance resistance was affected more significantly by the surface texture and shapes. The signal inductive resistance of subsurface was increased at different levels. The phase comparison between surface and

subsurface defects at different rail sections indicated the measurement results were affected by defect locations and also the surface shape and textures.

Recommendations

From this investigation, the machined cracks in steel samples and surface/subsurface defects in rail samples were measured based on the improved real-time EC inspection system. Some recommendations can be provided as follows:

(1) Within the effective penetration depth, the improved EC system could be used to identify crack severity during rail inspection. The impedance magnitude and phase plots showed the consistence trend with the changed crack depths and sizes in machined samples and rail tracks. Especially, the induction resistance and reactance decrease with the increasing crack depths.

(2) The developed EC system have the ability to detect different surface/subsurface defect types on rail samples and to identify the defect depth or location effects. Generally, the induction resistance decreased with the defect depth. The subsurface crack can contribute to the inductive reactance. These results can help to classify the defect types on rails.

(3) Subsurface defects can be detected with the improved EC system with a relatively large effective penetration depth at rail head, rail gauge corner, and rail web. In addition, the normalized impedance showed distinct characterizations compared with that of surface cracks at different locations. The comparison should be conducted within the rail section with similar flawless surface conditions. Some known steel samples will be collected to test the subsurface defects with the system. These results can be potentially used for the validation of subsurface defect detection.

(4) The distance between the sensor and the measuring surface needs to be investigated with different excitation amplifier voltages. Even though the penetration depth is constant when the excitation voltage changes, the intensity of the eddy current magnetic field in the rail sample will be changed. The suitable sensor working distance should be selected to obtain the sensitive inductive signals with different excitation amplifier voltage levels. The working distance is also critical to avoid the sensor damage with uneven rail surface.

Overall, the developed EC detection system can achieve good sensitivity for different defect measurements of both machined lab samples and collected rail samples by considering defect severity and geometry changes. More rail sample measurements need be conducted to evaluate the capacity of EC detection system on defect classification and geometry parameter identification.

Contacts

Principal Investigator
Pasi Lautala, Ph.D., P.E.
Associate Professor
Director, Rail Transportation Program
Department of Civil and Environmental Engineering
Michigan Technological University
(906)-487-3547
Email: ptlautal@mtu.edu

NURail Center
217-244-4999
nurail@illinois.edu
http://www.nurailcenter.org/

References

1. *https://www.olympus-ims.com/en/ec-probes/spot/#!cms[focus]=cmsContent10678.*
2. García-Martín, J., J. Gómez-Gil, and E. Vázquez-Sánchez, *Non-destructive techniques based on eddy current testing.* Sensors, 2011. **11**(3): p. 2525-2565.
3. Sophian, A., et al., *Electromagnetic and eddy current NDT: a review.* Insight, 2001. **43**(5): p. 302-306.
4. Beretta, S., et al., *Corrosion–fatigue of A1N railway axle steel exposed to rainwater.* International Journal of fatigue, 2010. **32**(6): p. 952-961.
5. Gao, Y., et al., *Multiple cracks detection and visualization using magnetic flux leakage and eddy current pulsed thermography.* Sensors and Actuators A: Physical, 2015. **234**: p. 269-281.
6. Song, Z., et al., *Detection of damage and crack in railhead by using eddy current testing.* Journal of Electromagnetic Analysis and Applications, 2011. **2011**.
7. Pohl, R., et al., *NDT techniques for railroad wheel and gauge corner inspection.* NDT & e International, 2004. **37**(2): p. 89-94.
8. Kapoor, A., I. Salehi, and A.M.S. Asih, *Rolling Contact Fatigue (RCF)*, in *Encyclopedia of Tribology*, Q.J. Wang and Y.-W. Chung, Editors. 2013, Springer US: Boston, MA. p. 2904-2910.
9. Mayville, R., P. Hilton, and D. Peirce, *Investigation of rail bolt hole cracks*. 1987.
10. Rifai, D., et al., *Subsurface defects evaluation using eddy current testing.* Indian J. Sci. Technol, 2016. **9**: p. 10.17485.
11. He, Y., et al., *Eddy current pulsed phase thermography for subsurface defect quantitatively evaluation.* Applied Physics Letters, 2013. **103**(14): p. 144108.
12. Placko, D. and I. Dufour. *Eddy current sensors for nondestructive inspection of graphite composite materials*. in *Conference Record of the 1992 IEEE Industry Applications Society Annual Meeting*. 1992. IEEE.